Contribution of Analytical Microscopies to Human Neurodegenerative Diseases Research (PSP and AD)

Carmen Quintana*

IMM-CNM, CSIC, 8 Isaac Newton, 28760 Tres Cantos, Madrid, Spain

Abstract: Using analytical microscopies we have observed an increase of Fe^{2+} iron-induced oxidative stress inside pathological ferritin (Ft). This finding, together with the presence of Ft in myelinated axons associated with oligodendrocyte processes and myelin sheet fraying, suggests that a *dysfunction of ferritin* (a ferritinopathy) may be the non-specific aging-dependent pathogenic event responsible for neurodegenerative disease.

Key Words: Ferritinopathy, neuropathology, alzheimer, analytical microscopies, nanoSIMS.

INTRODUCTION

An interesting theory states that neurodegenerative diseases (ND) can be explained by the combination of two pathogenic events: one specific and associated with the aggregation of a particular protein in the central nervous system (CNS), and the other non-specific and associated with aging and the production of an excess of free radicals [1].

Examples of particular proteins that aggregate are the hyper-phosphorylated tau protein in PSP, Pick and AD, the β-amyloid protein (β-A) in AD, the α-synuclein in Parkinson Disease, PrP in prion diseases, and Superoxide Dismutase (SOD) in lateral amyotrophic sclerosis (LAS).

The excess of free radicals leads to oxidative cellular damage in brain [2,3]. One important source of free radicals is the free ferrous iron, Fe^{2+}, and the hypothesis that some dysfunction of the iron metabolism in the human brain can be involved in the onset of ND has been reviewed by several authors in recent years [4-7]. In fact, iron accumulation in the brain has been observed since 1953 in neurological diseases including PSP and AD [8]. The disruption to the iron metabolism may occur at several levels: iron uptake and release, *storage,* intracellular metabolism and regulation [6].

Concerning storage, *ferritin (Ft)* is the main protein involved in iron storage [9]. Their physiological role is to accumulate the excess of iron in redox-inert forms, Fe^{3+}, in their central cavity (the core), where iron is mainly stored as hydrated Fe^{3+} iron oxide nanocrystals, Fig. (**1a**). The hollow protein shell ($d_{int} \approx 7$nm, $d_{ext} \approx 12$nm) is composed of 24 sub-units of varying composition, a heavy polypeptide Ft-H (MW ≈ 21 kD) and a light polypeptide Ft-L (MW ≈ 19 kD). The Ft-H and Ft-L sub-units have different physiological roles. Ft-H has a ferroxidase center that catalyses Fe^{2+} oxidation; it is predominant in organs requiring iron detoxification and cellular protection, such as the heart and brain. Ft-L facilitates mineralization.

Ferritin has been identified at a histological level in the pathological brain by immunohistological methods [10,11].

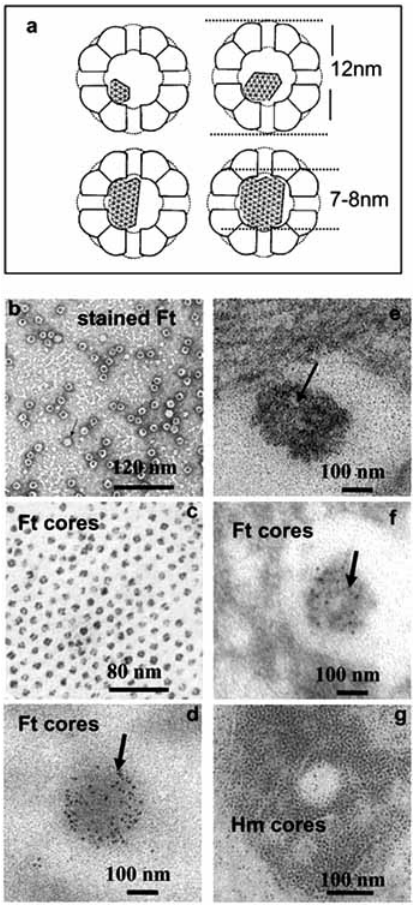

Fig. (1). Morphology of ferritin (Ft) and hemosiderin (Hm), (a) schema of the ferritin morphology, a spherical protein with an internal cavity (the core) where the iron is stored as hydrated iron oxide nanocrystals. (b) the protein shell of Ft is observed with negative uranyl acetate staining, (c) the cores of Ft are observed in unstained isolated molecules, (d) the Ft cores observed in unstained brain sections, (e) In uranyl acetate stained brain sections, the Ft cores are not visible, (f) the Ft cores are visible in lightly uranyl acetate brain stained sections, (g) Hm clusters in unstained section of mouse hepatocytes.

*Address correspondence to this author at Instituto Microelectronica de Madrid, Parque Tecnologici de Madrid, 8 Isaac Newton, 28760 Tres Cantos, Madrid, Spain; Tel: 34-91.8060700; E-mail: carmen@imm.cnm.csic.es

Using biochemical methods some mishandling of Ft has been observed in ND. For example, the increase in both H and L-subunits of Ft that occurs during aging, fails to occur in Alzheimer's disease [12]. A mutation in the gene encoding Ft-L is the cause of a neuroferritinopathy, a recently discovered neurodegenerative disease characterized by the presence of intranuclear and intracytoplasmic neuroferritin inclusions, and iron accumulation in the brain and other tissues [13-18]. *Direct* visualization of ferritin has been achieved through transmission electron microscopy (TEM) on *extracts* of aberrant Tau filaments in PSP [19] and on *extracts* of PHF in AD [20-22]. Ferritin has also been identified '*in situ*' on *sections* in PSP caudate nucleus [22] and in AD hippocampus [23].

Using analytical transmission electron microscopy (ATEM) methods such as high resolution transmission electron microscopy (HRTEM), electron nanodiffraction (END) and electron energy loss spectrometry (EELS), we have studied the core composition of these pathological ferritins. These techniques, which are currently used for nanoanalysis in Materials Science, are little known and rarely used in Life Sciences; but they have allowed us to identify the mineral phases of nanocrystals forming the *individual* ferritin cores.

Significant differences in mineral composition between the physiological and pathological ferritin cores have been found [21,22]. Whereas the major mineral phase in physiological ferritin is similar to 6L-ferrihydrite, one ferric (Fe^{3+}) iron oxide, in pathological ferritin the major mineral phases are two cubic phases, a magnetite-like phase and a cubic a=0.43nm phase in which *ferric and ferrous* iron ions are present. In addition, there is a high degree of similarity between these cubic a=0.43nm phase and the poorly crystallized phase of hemosiderin (Hm) cores. Hemosiderin, the second iron-storing molecule, is considered to be a partial proteolytic product of ferritin and is present in pathological iron overload (hemochromatosis and siderosis).

Ft and Hm were visualized in damaged brain regions of PSP and AD patients [22,23]. In AD, Ft was observed in the coronal region of the senile plaques associated to a non-β-amyloid component and in the periphery of plaques, together with Hm, in sulfur-rich dense bodies of dystrophic neuritis. Ft was found to be particularly abundant in dystrophic myelinated axons in association with oligodendrocytes processes. In glial cells of both AD and PSP patients Ft was observed in the nucleus and cytoplasm and Hm was found in lysosomes-siderosomes.

These findings provide new arguments to support the previously proposed hypothesis [21] that a dysfunction of ferritin is associated with PSP and AD (with eventual degradation to Hm) [22]. In fact, a defect in the enzymatic oxidation of iron inside ferritin could be a cause of the increased concentration in the brain of toxic free ferrous (Fe^{2+}) iron, contributing to the production of free radicals that induce both cellular oxidative stress and aged-related myelin breakdown associated with cognitive decline and AD [24]. In short, a ferritinopathy, induced by genetic or non-genetic factors, could be one of the non-specific and aging correlated events that can contribute to the onset of PSP, AD and other NDs.

The present review aims firstly to show how the analytical microscopies led us to propose the above-mentioned hypothesis and secondly to put forward the applications of analytical microscopies in the neuropathological field.

MATERIALS AND METHODS

Sample Preparation

For analysis of physiological ferritin molecules commercial horse spleen (Calbiochem and Sigma) and human liver ferritin (Calbiochem) were used. The commercial solution is diluted in water (at about 1:100) and a drop of this diluted solution is placed on a carbon-coated copper or titanium grid.

Isolation of brain ferritin (PSP, AD and healthy subjects) was previously described [19]. A drop of the undiluted solution was placed on a carbon-coated copper, nickel or titanium grid.

Identification of Ft and Hm '*in situ*' was performed on brains of PSP and AD patients. The sample preparation has been described previously [22]. Briefly, fresh-frozen fragments of brain from autopsies of PSP, AD and healthy subjects were collected. Caudate nucleus and hippocampus fragments were obtained from PSP and AD subjects respectively. The fragments were thawed in a chemical fixative (4% paraformaldehyde and 1% glutaraldehyde in 0.4 M Hepes buffer (pH=7)), cut into fragments of about 3mmx 3mmx3mm that were fixed in the same fixative at room temperature for 12h. Samples were dehydrated in acetone (or ethanol) and embedded in Epon (or Lr-white) resin at 60ºC for 48h. Conventional thin sections of 40-60 nm were obtained and directly collected on copper or gold grids. For ultrastructural studies the sections were lightly stained with uranyl acetate 2% in water for 30 seconds.

The brain samples were provided by the 'Banco de Tejidos para enfermedades neurologicas', Madrid (Spain), the 'Netherlands Hersen Bank' (Dr. Ravid), (Netherlands), the 'Pitié-Salpetriére Brain Bank, Raymond Escourolle Neuropathology Department', Paris (France) and the 'Institute of Neuropathology Brain Bank', Hospital Universitari de Bellvitge, Hospitalet de Llobregat, Barcelona (Spain).

TECHNIQUES

Identification of Individual Ferritin and Hemosiderin Molecules in Biological Samples

TEM observation of biological samples is currently carried out on stained preparations; negative uranyl acetate staining (AcU) for the isolated molecules and uranyl acetate plus lead citrate staining for thin sections of tissues.

For isolated molecules placed on a carbon-coated grid, the negative uranyl acetate staining permits the observation of the protein hollow shell of the Ft, Fig. (**1b**). Visualization of the Ft cores in conventional bright field TEM can only be performed on *unstained* preparations; they appear as isolated dark precipitates of 5-8 nm in diameter, Fig. (**1c**) shows the cores of the horse spleen isolated Ft molecules and Fig. (**1d**) shows the cores of the Ft molecules present in AD brain sections; the minimal distance between the cores, 12-14nm, corresponds to the protein shell diameter. In unstained sec-

tions the cellular structures cannot be easily observed and in conventional stained sections the uranium and the lead precipitates make the observation of Ft cores difficult, Fig. (**1e**). One compromise solution is to lightly stain with AcU to allow both the visualization of Ft cores and cellular structures Fig. (**1f**).

Hemosiderin, the second iron storage molecule, is considered to be a partial proteolytic product of ferritin; consequently the cores are often visualized as clusters of dark particles in secondary lysosomes or siderosomes [25]. Fig. (**1g**) shows clusters of Hm in a siderosome of mouse hepatocytes.

Identification of the Mineral Phase in Crystals

Background

A crystal, Fig. (**2a**) is defined as a set of atoms or group of atoms (called a motif) placed on a 3D regular lattice of points (Bravais lattices), Fig. (**2b**). In the crystal it is possible to define *crystallographic planes* of lattice distances, d_i, Fig. (**2c**).

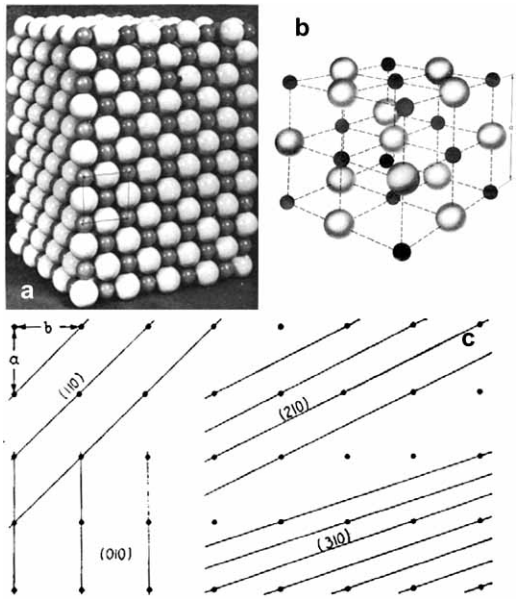

Fig. (2). (a) Model of a crystal, (b) elemental cell unit of a cubic face center (cfc) crystal composed of two types of atoms, (c) 2D projection of the crystallographic plans of cubic crystals.

Measurements of the lattice distances d_i, can be made by X-Ray diffraction (XRD) or electron diffraction (ED). Both methods use the Bragg law; when a beam of monochromatic X-ray photons or electrons interact with a set of crystals oriented in all spatial directions they are scattered by the crystal planes at discrete directions following the Bragg law :

$2.\ d_i.\ \sin\phi_i = n.\lambda$

d_i = distances between the crystallographic planes

λ =Wavelength of X-ray or electron

ϕ_i = Bragg angles

Fig. (**3a**), shows the schema of an X-ray diffraction system used to study a set of crystals oriented in all spatial directions (Debye-Scherrer or powder method); the diffracted X-ray at Bragg angles forms the '*diffraction pattern*' which is detected and measured with a suitable X-ray detector (photographic film or other); for a powder sample the 'diffraction pattern' is visualized, on a 2D detector, as a set of discrete rings. Fig. (**3b**) shows five powder X-ray diffractograms of different phases of an Al-Ni alloy recorded on photographic film (fp). By measuring the diffracted angles ϕ_i, the lattice distances, d_i, are determined. Each phase presents a characteristic set of the lattice distances, d_i.

Fig. (**3c**) shows the equivalent schema of an electron diffraction system; the object is, in this case, a monocrystal thin film and the diffraction pattern is now formed by discrete spots (the diffraction maxima) Fig. (***3e***).The relationship between d_i and the ray, R_i, is now

$R_i = \lambda L/d_i$

With L = camera length that must be calibrate with a reference sample

Fig. (**3d**), shows the formation of the selected area diffraction (SAD) pattern in the back objective lens of a TEM. Fig. (**3e-h**) show examples of the different SAD patterns that can be observed in a TEM; a monocrystalline sample, an amorphous sample and two polycrystalline samples of two different iron oxides (with two different set of d_i).

The position of the Bragg angles is determined only by the geometry of the lattice and not by the arrangement of atoms at each lattice point. Consequently*, the diffraction pattern contains information on the unit cell geometry and symmetry of the crystal*. In some cases (kinematical approximation) the relative intensities of the diffraction maxima should be used for the study of the crystal structure (number, position and distribution of atoms in the unit cell of the lattice).

To identify the mineral phase of a crystal the first step is to know its chemical composition (iron and oxygen in this case). The second step is to measure the lattice parameters and intensities by X-ray or electron diffraction and compare them with those of the known minerals, composed of the same chemical element - in the case of ferritin cores, the different iron oxides. For complex structures the procedure is to compare the calculated intensities of the modeling structures with the experimental ones.

For nanometer-size crystals, X-ray diffraction is not a useful method [26] because of the inverse relationship between the size of the diffraction maxima and the size of crystals (shape factor). Electron diffraction, especially electron nano-diffraction (END), constitutes a more adequate tool for the study of nanocrystals [27]. In TEM the selected-area diffraction can be used to obtain single crystal patterns from crystals a few tenths of a nm thick and with a typical lateral extension of about 50-100 nm. By using electron nanobeams such as those produced in analytical transmission electron microscopes (ATEM), the diameter of the analyzed specimen can be reduced to 1nm.

Identification of the Mineral Phase of Ferritin Cores from Electron Nanodiffraction

Electron nanodiffraction patterns of Ft cores can be obtained in an ATEM [28]. They are obtained through the fo-

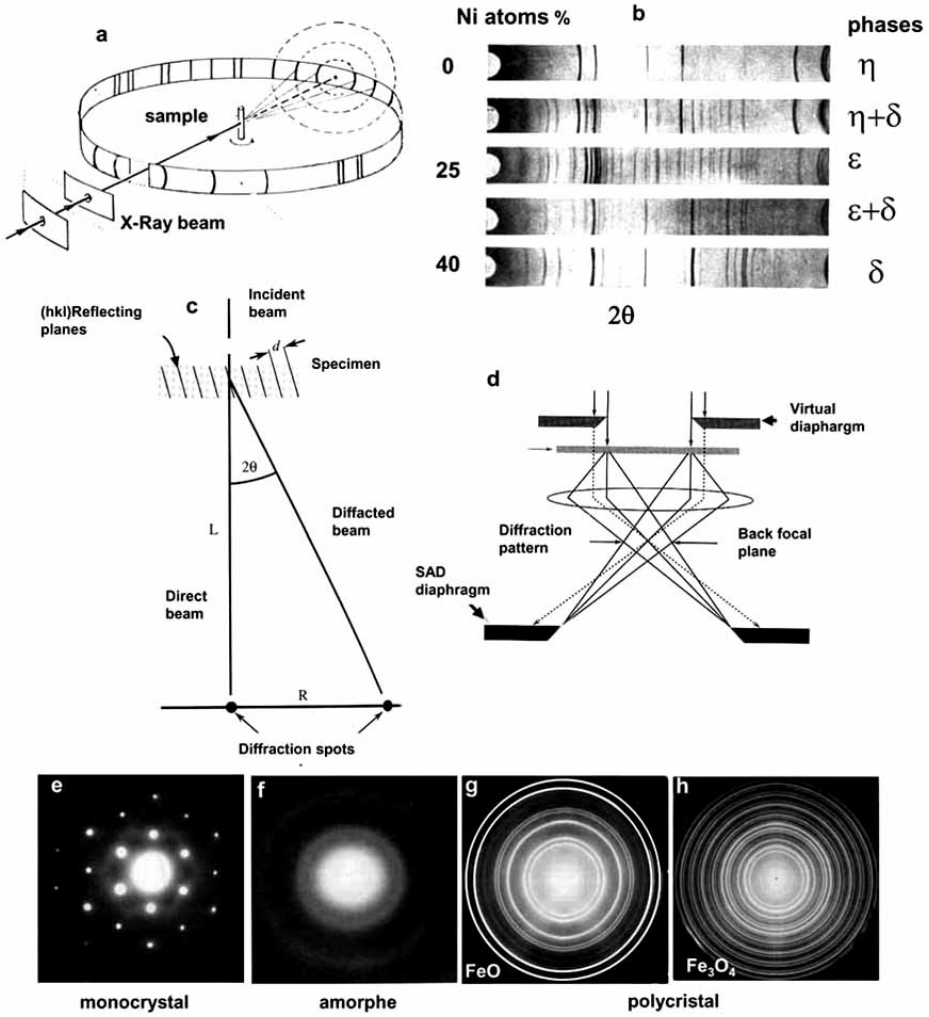

Fig. (3). (a) Schema of an X-ray diffraction system to study powder samples, (b) X-ray diffraction pattern of the five phases of Al-Ni alloy powder samples, (c) schema of an electron diffraction system to study thin films, (d) formation of the selected area diffraction (SAD) patterns in a TEM, (d) Different SAD patterns that can be recorded in a TEM, (e) monocrystal sample, (f) amorphous samples, (g-h) two different polycrystalline iron oxides.

calization of a parallel electron beam of nanometer diameter on the analyzed nanocrystal. The diffraction patterns, similar to SAD, are also recorded in the back focal plane of the objective lens. Figs. (**4a-b**), show an electron nanodiffraction pattern of a Ft core and the corresponding theoretical diffraction pattern [28]. Nanodiffraction patterns are more easily obtained in a dedicated STEM instrument where the beam diameter at the specimen level can be smaller than 0.7nm and large numbers of nanodiffraction patterns from individual crystals can be recorded rapidly. Figs. (**4c-d**) show an example of END and the corresponding theoretical diffraction pattern of a crystal of synthetic 2-L ferrihydrite [29].

END was used for the study of the mineral phases of physiological and pathological ferritin cores [22,30]. The experimental procedure was the following; when a bright-field or dark-field image of a high magnification ferritin molecule core is viewed on the display screen of the STEM, an electronic marker is placed on the image of the core. The beam is stopped at that point and the nanodiffraction pattern from the core is displayed on a TV monitor and either photographed directly or else stored on a video-cassette recorder (VCR), for future photography and analysis. Typically, a series of nanodiffraction patterns may be observed or recorded as the beam is translated across a core to detect any variations of structure. Since the crystallites in the ferritin cores come in an arbitrary orientation, many nanodiffraction patterns come from non-axial orientations and are difficult to interpret. However, in the case of two-dimensional single-crystal patterns coming from crystallites which are close to an axial orientation, comparisons of the dimensions and relative intensities with those for patterns calculated for known structures are usually sufficient to allow the phase to be identified without ambiguity.

Identification of the Mineral Phase of Ferritin Cores from High Resolution Transmission Electron Microscopy Images (HRTEM) and Fourier Transform (FT)

HRTEM images recorded under specific conditions of defocus are closely related to the projection of the atomic potential distribution of the crystal and it can be considered

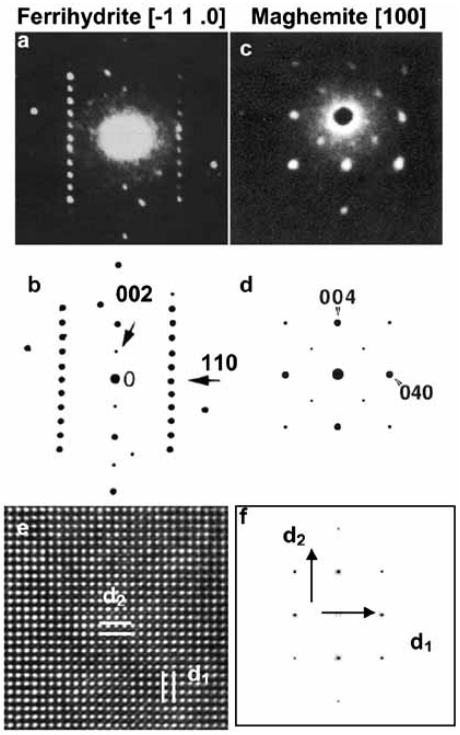

Fig. (4). (a-b) electron nanodiffraction pattern (END) of one hexagonal ferrihydrite crystal in [-11.0] orientation and the corresponding theoretical diffraction pattern, (c-d) electron nanodiffraction pattern (END) of one cubic maghemite crystal in [100] orientation and the corresponding theoretical diffraction pattern, (e-f) HRTEM of a cubic InP thin film monocrystal in [100] orientation and the corresponding digital diffractogram; the module of vectors $\mathbf{d}_1$ and $\mathbf{d}_2$ provide the measure of lattice distance of {002} plans, $d_{002}=d_{020}=$ 0.295nm.

that the periodicities of interference fringes represent the lattice spacing, Fig. (**4e**). When the crystal is oriented with a simple zone axis parallel to the electron beam, the HRTEM images show at least two systems of fringes from which two lattice spacings can be derived. If the measured lattice spacing differs from one mineral phase to the other, then the identification is unambiguous. The measurement of fringe periodicities in HRTEM can be performed more precisely by computing the numerical Fourier Transform of HRTEM images to obtain the digital diffractogram, Fig. (**4f**). In this case the intensities of the maxima cannot be used for the study of the crystal structure.

Compositional Data

The TEM high contrast of the ferritin cores is essentially due to the presence of the iron, a chemical element, heavier that the biological elements (H, C, O, and N) that constitute the protein shell. However, precipitates of other heavy elements can produce similar contrast; as is the case, in conventional staining, with uranium and lead precipitates. Consequently it is necessary to perform an '*in situ*' chemical microanalysis to verify the presence of iron in the observed cores of Ft. Chemical microanalysis can be performed using X-ray, Fig. (**5a**). EELS associated to TEM, Fig. (**5b**) and by SIMS (secondary ion mass spectrometry). The X-ray and EELS methods allow the identification of the compositional elements of the nanocrystals; oxygen and iron in the case of ferritin cores. EELS also permits us to know the valence state of the iron oxide that composes the ferritin cores; Fe^{3+} and/or Fe^{2+} states, Fig. (**5c**) [31]. Again, with STEM instruments the analysis can be made on an individual molecule Fig. (**5d**).

SIMS allows direct identification of chemical elements and isotopic analysis with high sensitivity and specificity, Fig. (**6a**). SIMS microscopy is a secondary ion emission image method permitting the visualization and mapping of the chemical distribution of an object surface. The latest generation of SIMS instruments, the NanoSIMS 50 microscope works in scanning mode and can be used to map the compositional elements at subcellular level [23,32,33], Fig. (**6b**).

Standards

We have used synthetic magnetite, Fe_3O_4, and commercial horse spleen ferritin (Calbiochem and Sigma) as standards. The solutions of synthetic magnetite and commercial ferritin were diluted at 1:100 and a drop of the solution was placed on a carbon-coated copper grid.

Instruments

An HRTEM 200-kV Hitachi HF2000-FEG was used to obtain high resolution images at high magnification (G = 7.10^5 and 1.10^6). The limiting point resolution obtained with this microscope is 0.13nm. This microscope is equipped with a CCD Camera (MSC 794 Gatan). High resolution images were digitally acquired with the CCD Camera at 1024x1024 or 512x512 pixels x2 bytes, using either an objective aperture of 160 µm, or without an aperture. The Fourier Transform (FT) was computed with Digital Micrograph software version 2.5 on a Power Mac or with CRISP software on a PC after conversion to one byte. Calibrations of FT at several magnifications were made on high resolution images using an Al sample. Pixel sizes were 0,0265 nm for $G=7.10^5$ and 0,0210nm for $G= 1.10^6$. Filtered images (inverse FT) were performed with CRISP software. The indexing of the power spectrum (PS) (square of the modulus) of the Fourier Transform intensities (digital diffractogram) and the computation of diffracted intensities for each structural model of Fh were performed with the aid of Electron Diffraction software version 6.8 (Mornirolli, University of Lille) for PC.

Electron nanodiffraction patterns were obtained with a dedicated scanning transmission electron microscope, the HB-5 from VG microscopes, Ltd., specially modified for the observation and recording of electron nanodiffraction patterns and equipped with TV-VCR and CCD recording systems.

X-ray nanoanalysis was performed using a FEG-200kV Jeol 2010. With this instrument, it is possible to obtain a significant Kα-Fe signal of 2-3 core of ferritin.

EELS spectra were acquired with a FEG-200kV PhilipsCM200 equipped with PEELS and Gatan image filter GIF-200, a CCD camera (MSC 794 Gatan) and Digital Micrograph version 2.5 and EL/P 3.0 software working on a Power Mac. The spectra were acquired in TEM mode, with an energy dispersion of 0.3 eV/channel, an acquisition time

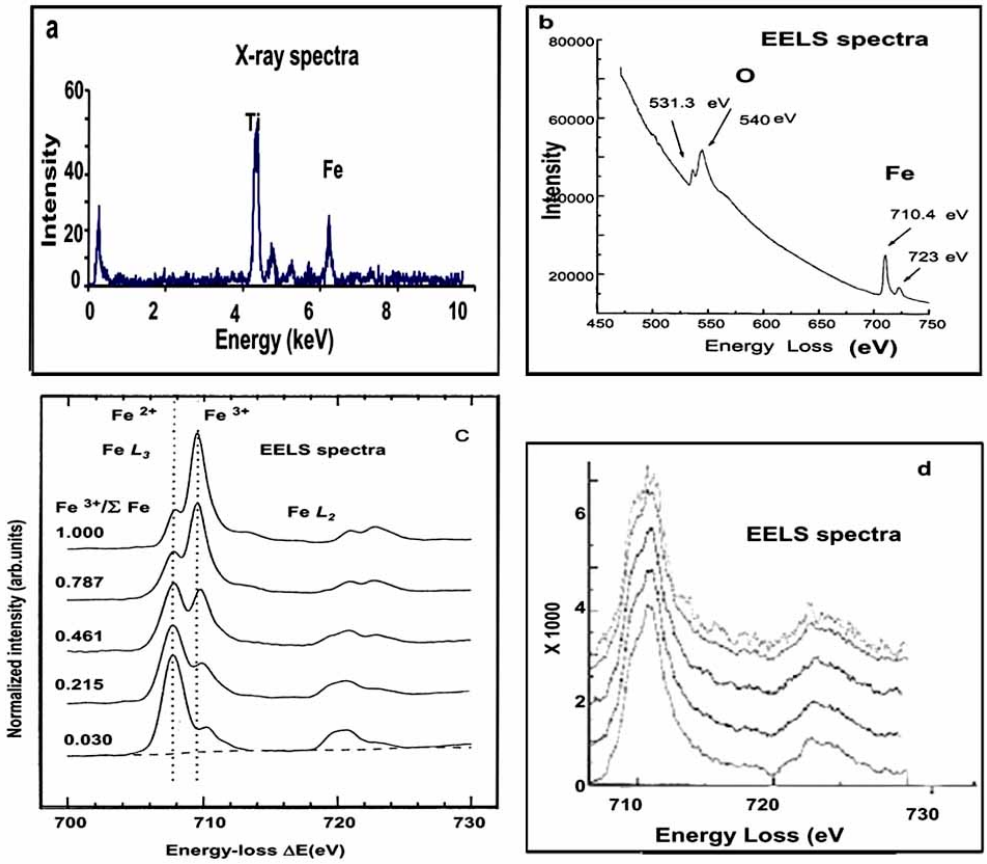

Fig. (5). (a) X-ray spectrum of a set of 2-3 Ft molecules, (b) EELS spectrum of set of 5-6 Ft molecules, (c) high energy resolution EELS spectra of a set of iron oxides; the fine structure of the $L_{2,3}$ peak is dependant of the valence state of iron oxides (according to [31]), (d) EELS chrono-spectra of an individual Ft molecule showing that the composition does not change with the dose of electron irradiation; the form of the $L_{2,3}$ peak suggests the presence of a mixed Fe^{2+}-Fe^{3+} iron oxide. (courtesy of A. Gloter).

of 3 sec and, in each point, 20 spectra were co-added. The spectra were background substrated using the Egerton power law and following this procedure, white lines $L_{2,3}$ of iron were fitted with 2 or 3 Lorentzian curves and the following characteristic parameters were defined and computed: distance between peak maxima, width and height of L_3 and L_2 peaks, and ratio of L_3 or L_2 peaks areas or heights. With this instrument, it is possible to obtain a significant $L_{2,3}$ signal of 5-6 core of ferritin.

EELS analysis of some individual ferritin cores was performed with an HB-501 STEM from VG instruments.

RESULTS

Composition of Ferritin Cores

Background

Identification of the mineral phase in ferritin cores was first performed in the 1960s on ***a set*** of molecules. At that time, the accepted mineral composition was similar to the natural mineral described as *ferrihydrite (Fh),* [34]. Characterization of this material is difficult because it occurs only in a nanocrystalline state. Several models of ferrihydrite structure were proposed [34-36]. The model of Harrison, Fischbach, Hoy and Haggis [35], and the model of Towe and Bradley [34], are based on X-ray diffraction (XRD) and selected area electron diffraction (SAD). Both models are three-dimensional with a hexagonal lattice. In the Harrison, Fischbach, Hoy and Haggis model, the parameters are a = 0.294 nm and c = 0.94 nm and in the Towe and Bradley model the parameters are a = 0.508 nm and c = 0.94 nm; the difference between the two models is due to the position of iron between the layers of oxygen. The model of Heald, Stern and Bunker [36], is related to EXAFS measurements of molecules in a solution. The model is two-dimensional and can be described as a hexagonal structure of a = 0.33 nm and c = 0.46 nm. The dark field TEM images of Massover and Cowley [37] as well as the electron microdiffraction in STEM obtained by Isaacson and Othsuki [38] and the electron nanodiffraction in TEM obtained by Quintana, Bonnet, Jeantet and Chemel, [28] support the three-dimensional model of Towe and Bradley [34].

Two decades later [39-41], *ferrihydrite* raised industrial interest and led to the synthesis and analysis of new preparations of Fh to be studied by different analytical techniques: EXAFS, XANES and Môssbauer spectroscopy, isotopic exchange and structural modeling of X-ray diffraction patterns (for a review, see [41]. To sum up, two forms of mineral have been described: the 6-line (6-L) form because the X-ray

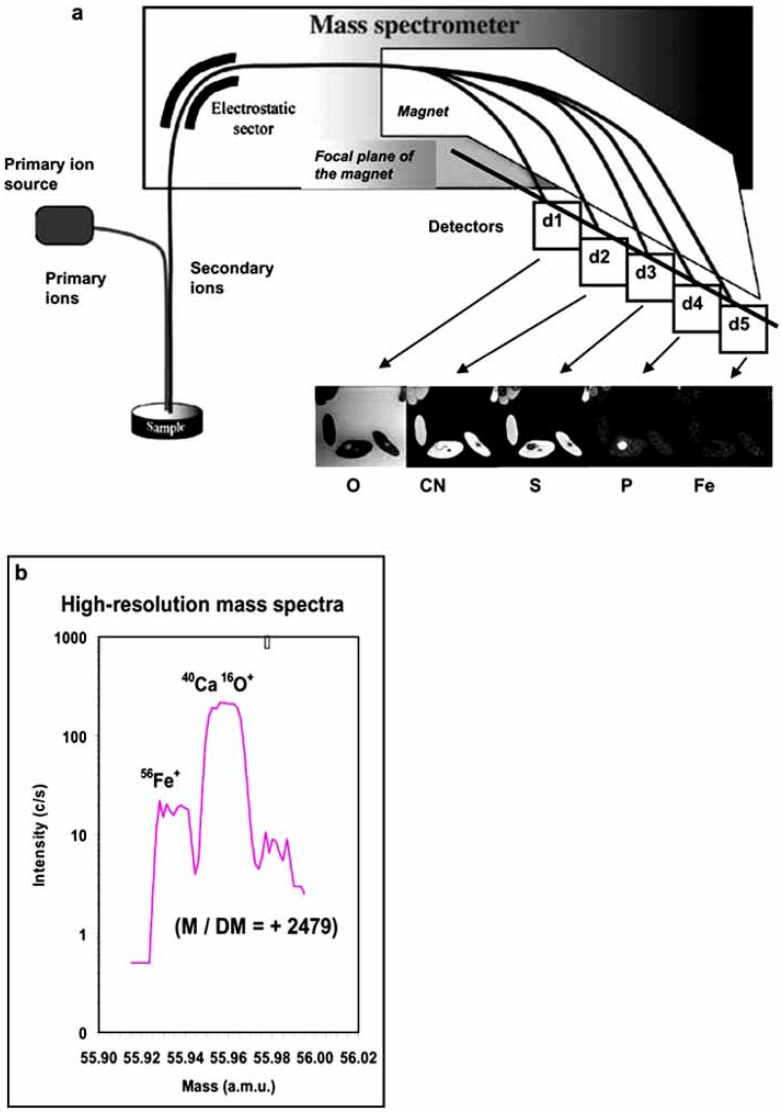

Fig. (6). (a) Schema of the NanoSIMS instrument equipped with five ion detectors to allow the recording of five different element maps at the same time (O, CN, P, S and Fe maps of sectioned quail erythrocytes), (b) High resolution mass spectrum at nominal 56 a.u.m. ($^{56}Fe+ {}^{40}Ca^{16}O$) recorded on a brain glial cell.

diffraction pattern contains only 6 lines and the 2-line (2-L) form because the X-ray diffraction pattern contains only 2 broad lines, Fig. (**7**). The difference between the two forms has been interpreted as being caused by the difference in crystal size. The structure proposed for the 6-L form is a hexagonal structure with a= 0.30 nm (or 0.56 nm) and c=0.94 nm) [40].

Several years later Janney, Cowley and Buseck [29,42] using END showed that both forms of Fh give single crystal patterns from individual nanocrystals. Furthermore they found a multiphase composition of both forms. In the case of the 6-L form, besides a hexagonal structure that was similar but not identical to that proposed by the X-ray data, they found other iron oxide phases such as hematite, maghemite-magnetite and wüstite. 2-L material shows different phases to 6-L material; one hexagonal phase but with a different structure to that in the 6-L material and a greater proportion of maghemite-magnetite.

The new studies on Fh demand a revision of the structure of ferritin cores obtained using updated techniques such as nano-analytical microscopies.

New Results on the Structure of Ferritin Cores Obtained with Nano-Analytical Techniques

Horse Spleen and Human Liver Ferritin

In 2000, two independent works using electron nanodiffraction [30] and high resolution transmission electron microscopy and electron energy loss spectroscopy [21] and a later joint work [22] on isolated horse spleen and human liver ferritin cores showed that the physiological Ft cores have a *mineral multiphase composition* very similar to 6-L Fh, with the major phase being the hexagonal one (Table **1**).

Brain Ferritin

Ferritin has been identified in normal and pathological brains since 1990 by immunohistological methods [10,11].

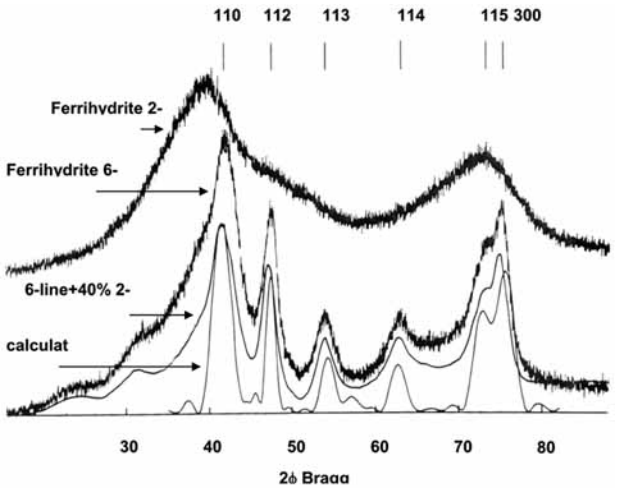

Fig. (7). X-ray diffraction of a set of Ft molecules allowing the identification of the mineral structure of the cores as a mixture of 6-line and 2-line ferrihydrite (from Eggleton and Fitzpatrick, [39]).

In 1998 Perez, Valpuesta, Montejo de Garcini, Quintana, Arrasate, Lopez-Carrascosa, Rabano, Garcia de Yebenes and Avila, [19] reported the presence of 'dense particles' associated with isolated aberrant TAU filaments in PSP patients, Fig. (**8a**). Similar observations were noted with PHF isolated from AD patients [20,21], Fig. (**8b**). In both cases they were identified as Ft cores.

The study of the core composition of these "pathological" Ft molecules was carried out using HRTEM, EELS and END [21,22]. The main results are summarized as follows:

1.- The ferritin cores from a diseased brain also have a *multiphase composition* but the most common phase is not the hexagonal phase but two cubic phases: a magnetite-like phase and a face-centered cubic phase with a = 0.43 nm, similar to wüstite and with strong faulting (Table **1**).

Fig. (**9**) and Fig. (**10**), show examples of these different phases. Figs. (**9a-d**), show the HRTEM image and the calculated digital diffractogram of a nanocrystal indexed as [00.1] 6L-ferrihydrite. Figs. (**9c-f**), show the HRTEM image and the calculated digital diffractogram of a nanocrystal indexed as [1-1.0] 6L-ferrihydrite; this crystal orientation, similar to

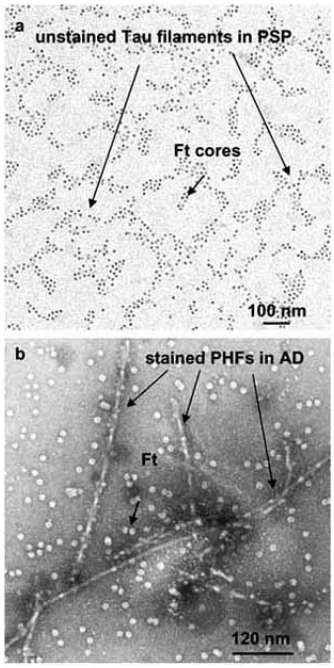

Fig. (8). (a) Ft cores associated to the aberrant TAU filaments isolated from PSP patients, (b) Ft molecules observed in negative stained preparations of isolated PHF from AD patients.

that shown in Fig. (**4a**), permits the *c* parameter (deduced from the (004) reflexion) to be measured. In Fig. (**9b-e**), the HRTEM image and the calculated digital diffractogram a nanocrystal indexed as [48.1] hematite is shown.

Figs. (**9g-h**), show the HRTEM image and calculated digital diffractogram of a crystal showing a quasi-quaternary symmetry and Fig. (**9i-j-k**), display three possible indexations of this crystal: (***i***) as cubic magnetite in [251] orientation, (***j***) as cubic greigite in [100] orientation and (***k***) as hexagonal hematite in [24.1] orientation. Table **2** summarizes the experimental and theoretical lattice distances and the angles between the crystallographic planes.

Fig. (**10a**), shows an END pattern of a cubic a = 0.85 nm [001] nanocrystal and Figs. (**10b-c**), display the HRTEM

Table 1. Phases of Nanodiffraction Patterns Identified for Various Ferritin Sources: Bold Numbers Represent the Number of Identified Patterns; Numbers in Brackets are Percentages of Total Numbers (%)

Phase	Human Brain Pathological Ferritin (PSP + AD)	Horse Spleen and Human Liver Physiological Ferritin	Aged Human Brain Ferritin
6LFh hexagonal	26 (15)	33 (52)	26 (49)
Magnetite-like	57 (33.5)	19 (30)	10 (19)
fcc, a=0.43nm	90 (41)	3 (5)	14 (26)
Hematite	4 (2)	3 (5)	0 (0)
Minor phases	13 (8)	5 (8)	3 (6)

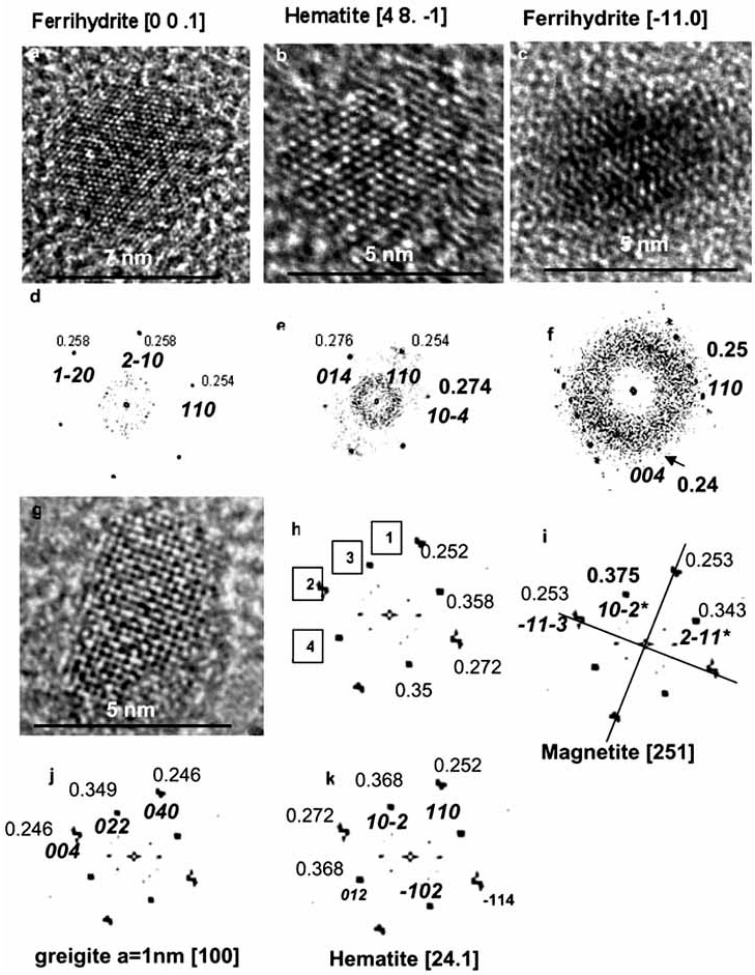

Fig. (9). Analysis of core nanocrystals of pathological Ft by Analytical Microscopies. (a-d) HRTEM image and digital diffractogram of one hexagonal ferrihydrite crystal in [00.1] orientation, (b-e) HRTEM image and digital diffractogram of one hexagonal hematite crystal in [48.1] orientation, (c-f) HRTEM image and digital diffractogram of one hexagonal ferrihydrite crystal in [-11.0] orientation, (g-h) HRTEM image and digital diffractogram of one nanocrystal with a quasi-quaternary symmetry, (i, j, k) three possible indexations of this crystal, (i) as cubic magnetite in [251] orientation, (j) as cubic greigite in [100] orientation and (k) as hexagonal hematite in [24.1] orientation (see Table **1**).

image and the calculated digital diffractogram of a cubic a = 0.85 nm [111] oriented nanocrystal, corresponding to a magnetite/maghemite phase. In Fig. (**10d-e**), two END patters of cubic a = 0.43 nm [001] and [110] oriented nanocrystals are shown.

Maghemite (γ-Fe_2O_3), is not readily distinguished from magnetite (Fe_3O_4) in HRTEM images or END patterns, because both have a similar structure, a cfc structure with a parameter of 0,8347nm and 0,8396 nm respectively. As magnetite is a mixture of Fe^{2+} and Fe^{3+} ions and maghemite contains only Fe^{3+} ions we have performed EELS analysis to differentiate both phases. Fig. (**10f**), shows the EELS spectrum recorded on isolated PSP Ft cores and Fig. (**10g**), the EELS spectrum corresponding to synthetic magnetite crystal. The energy resolution of these EELS spectra do not permit the fine structure of the L3 peaks, Fig. (**5c**), to be resolved but the shape of this peak and the similarity of the ratio L_3/L_2 shows the presence of magnetite in the Ft cores.

2.- The face-centered-cubic structure with a = 0.43 nm is similar to that detected in Hemosiderin (Hm) cores in primary hemochromatosis (Dickson 1998) [43]. Hm is present in pathological iron overload, as is the case of hemochromatosis and siderosis. Hemochromatosis and Ft accumulation in brain are considered risk factors for AD [44-46].

'In Situ' Identification of Ft and Hm in PSP and AD

With the aim of verifying '*in situ*' the presence of iron, Ft and Hm in brain regions affected by ND were observed at the subcellular level in the caudate nucleus of PSP patients and in the hippocampus of AD patients [22,23].

The main results were:

I.- Ferritin is observed in the pathological brain:

IN AD and PSP

- in the nucleus, cytoplasm and lysosomes of glial cells.

IN AD:

1.- in the *coronal region of SPs* associated to a non-β-amyloid component, Fig. (**11a-b**),

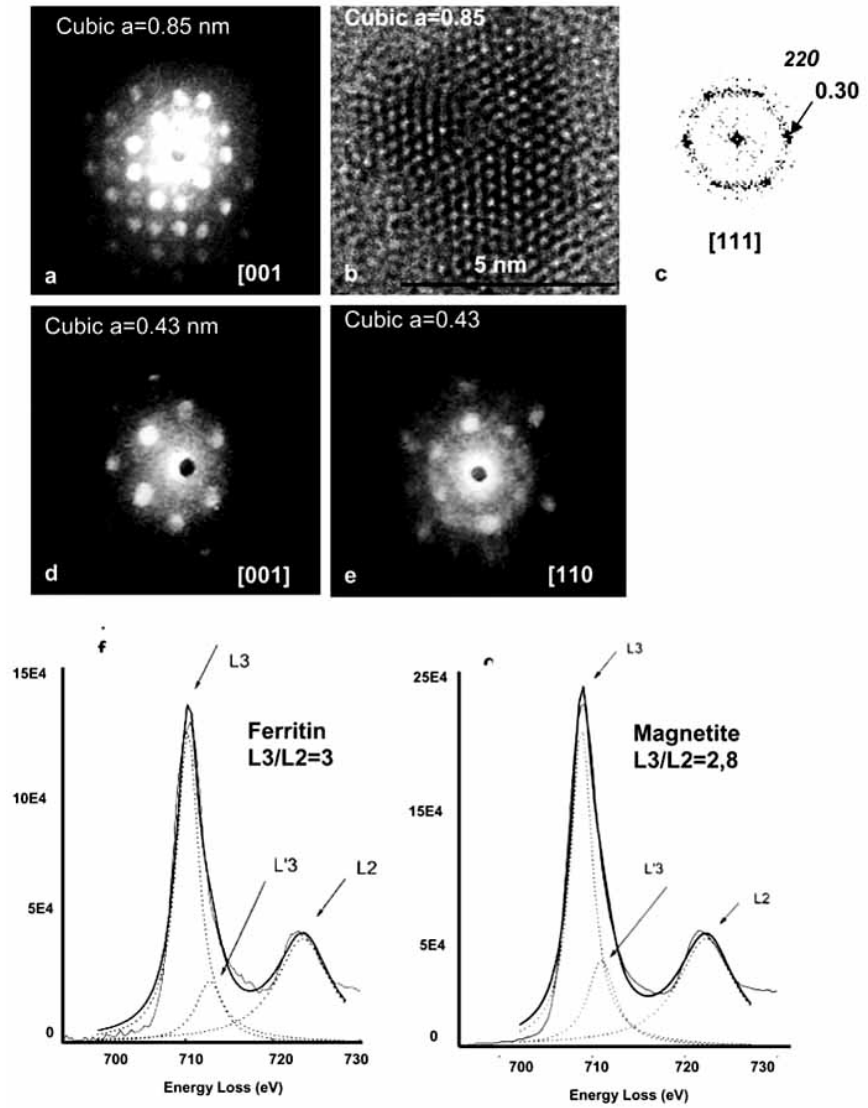

Fig. (10). (a-c) END, HRTEM and their corresponding digital diffractogram of two cubic a= 0.85nm (magnetite/maghemite) core nanocrystals of pathological Ft, (d, e) END of two cubic a=0.43nm core nanocrystals of pathological Ft, (f-g). Identification of magnetite by EELS, (f) EELS spectrum of a set of PSP Ft cores; (g) EELS spectrum of synthetic magnetite; the L_3/L_2 ratio of the PSP Ft cores is similar to L_3/L_2 ratio of the synthetic magnetite.

2.- in the *periphery of SPs* on the dystrophic neurites (DN) Fig. (**11c-d**),

3.- in *dystrophic myelinated axons* in association with oligodendrocyte processes and fryed myelin sheet Fig. (**12a-b-c**),

4.- we have not observed Ft, associated to PHFs, in neurons Fig. (**12e**),

II.- Hemosiderin is observed in the pathological brain.

IN AD and PSP

- in lysosomes-siderosomes and in cytoplasm of glial cells Fig. (**12d**),

IN AD

- in the periphery of SPs on the dystrophic neurites Fig. (**11d**),

Maps of cellular constituent elements O, C, N, S and P, Fig. (**13b, c, d**), and maps of Fe (see Fig. (**3**) in [23]) were obtained with the NanoSIMS 50 microscope at subcellular level. We have found that all the iron-rich regions mapped coincide with the Ft (or Hm) rich region observed in TEM, i.e. the cytoplasm and nucleus of glial cells and in the dystrophic neurites (DN) at the periphery of SPs. It is worth noting that in these latter regions *Fe is correlated with S*. Consequently, the NanoSIMS-detected iron is that which is contained in Ft (or Hm) cores.

DISCUSSION

Analytical electron microscopies allow us to produce new arguments to support the hypothesis that some dysfunction of the iron metabolism in human brain could be the non-specific aging-dependant factor associated with ND. The dysfunction of the iron metabolism could be a *dysfunction of*

Table 2. Phase Identification of the Quasi-Quaternary Symmetry Nanocrystals

Reflexions		**Magnetite/maghemite a=0.84nm <251>**		**Greigite a~0.986 <100>**		**Hematite a=0.503 c=0.137 <24.1>**	
	d_{exp}	d_{hkl}	hkl	d_{hkl}	hkl	d_{hkl}	hkl
1	0.252	0.253	3-1-1	0.246	004	0.252	110
2	0.272	0.253	-11-3	0.246	040	0.270	-114
$\alpha_{1,2}$	90	86		90		90	
3	0.353	0.375	01-2*	0.349	220	0.368	012
4	0.358	0.343	2-11	0.349	2-20	0.368	10-2
$\alpha_{3,4}$	86	90		90		86	

* forbidden reflexion in the cfc crystals

ferritin, i.e. a ferritinopathy induced by genetic or non-genetic factors. In effect ATEM allows us to show the *increase of ferrous iron inside pathological ferritin* consequently to the increase of mineral cubic phases, magnetite (in which ferric and ferrous ions are both present), and wüstite (a ferrous ion iron oxide).

The physiological task of ferritin is to protect cells from the redox active iron (Fe^{2+}). The ferrous ion is confined to and stored in the redox-inert form of Fe^{3+} in the molecular core. Under normal conditions the response to a cytosol increase in the production of redox-active iron (Fe^{2+}) is the rapid uptake of iron into the pre-existent ferritin cores. New Ft is then synthesized under the control of the iron itself. The presence of *ferrous* iron inside pathological ferritin could mean that the mineralization process is perturbed, for example that the enzymatic oxidation of iron inside ferritin is faulty [21,22]. The absence of Hematite (which is highly stable), the replacement of ferrihydrite by a magnetite and wüstite phases are consistent with an easier mobilization of

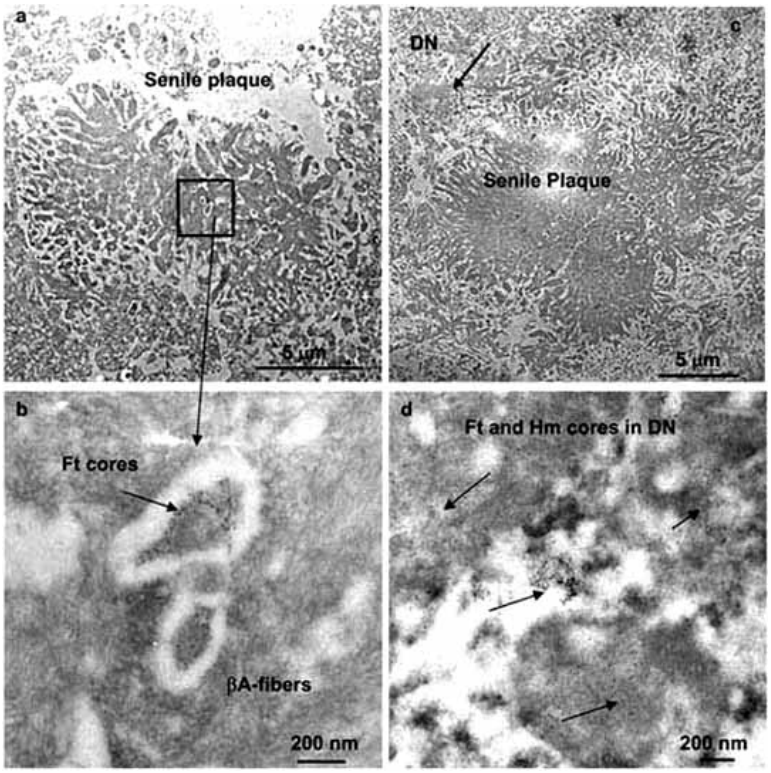

Fig. (11). TEM images of hippocampus sections of AD patients, (a) coronal region of a senile plaque, (b) detail of inset region of (a) showing Ft between the β-amyloid protein fibers (Ft is associated to a non β-amyloid SP compound [23], (c) central and coronal region of a senile plaque; in the periphery of SP's dystrophic neuritis (DN) (arrows) can be observed, (d) detail of a DN showing isolated ferritin cores and clusters of hemosiderin.

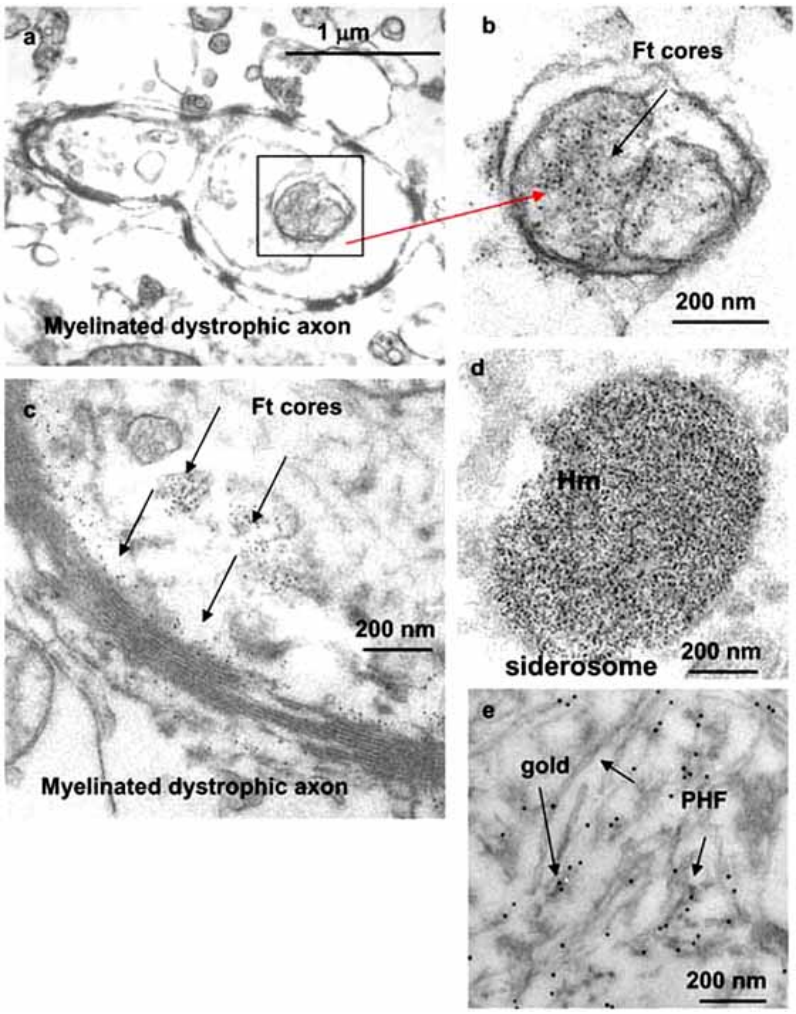

Fig. (12). TEM images of hippocampus sections of AD patients, (a) myelinated dystrophic axon in neuropilin showing Ft cores, (b) detail of the inset region of (a): high Ft concentrations are observed in oligodendrocyte processes, (c) Ft cores within myelin frayed sheets, (d) lysosome-siderosome filled with Hm in the cytoplasm of a glial cell, (e) immunogold staining of neurofibrillary tangles (NFT) with AbPHF-1 (gold of 10nm size); Ft are not associated '*in vivo*' to PHF filaments.

iron in these abnormal ferritins. The increase of unbound ferrous ions in cytoplasm may contribute to the production of free hydroxyl radicals that induce cellular oxidative stress.

Ferritin dysfunction has been previously reported in ND. A modified balance of H/L isoferritins is found in Parkinson and AD diseases [12]. Mutation of the gene that encodes the L ferritin subunit polypeptide is the cause of a neuroferritinopathy, a recently discovered neurodegenerative disease characterized by the presence of intranuclear and intracytoplasmic neuroferritin inclusions, and iron accumulation in brain and other tissues [13-18]. Oxidation of Fe^{2+} inside ferritin molecules takes place in specific ferroxidase sites in the Ft-H subunit [9]. However, it should be noted that genetic mutations associated to Ft-H subunit have not been described.

'*In situ*' studies of damaged regions in PSP and AD subjects have led us to observe the presence of significant amounts of ferritin and hemosiderin in several subcellular areas. According to previous observations [10,11], Ft is present in glial cells and in senile plaques but the greater amount of Ft is found in myelinated axons [23]. The "direct" observation of molecules allows us to specify the presence of Ft in the nucleus as well as the presence of Ft and Hm in lysosomes-siderosomes of glial cells. In senile plaques, Ft is present in the coronal region associated with a non β-amyloid compound and Ft and Hm are present in their periphery associated to sulphur. Consequently the presence of greigite, a magnetic $Fe^{2+}Fe^{3+}{}_2S_4$ mineral cannot be excluded [47,48]. We have not observed Ft or Hm in neurons.

The regions where the Ft molecules are particularly abundant are the myelinated axons in association with oligodendrocyte processes and within the frayed lamellae of myelin sheaths. Accumulations of Ft in oligodendrocytes can be interpreted two ways:

* Oligodendrocytes, the cells that produce the myelin, have the highest iron content of all brain cell types, and as much as 70% of brain iron is associated with myelin. Accumulations of Ft in oligodendrocytes could correspond to the general task of Ft as a cellular protector (iron detoxification).

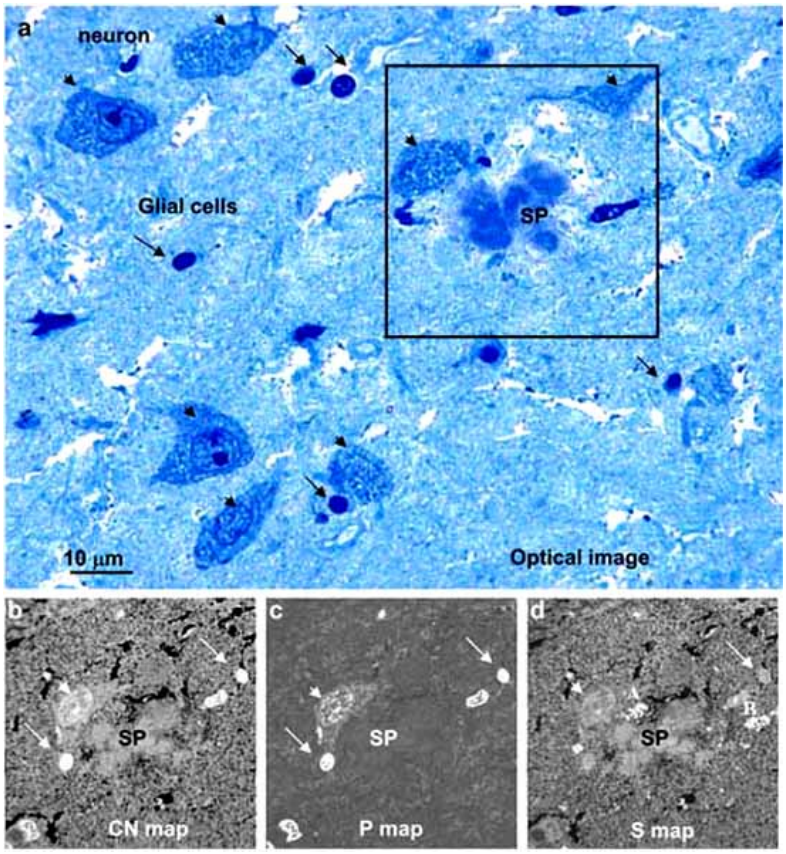

Fig. (13). (a) Optical image of a semi-thin section of AD hippocampus stained with toluidine blue. Neurons (arrowheads), glial cells (arrows) and senile plaques can be observed, (b-d) NanoSIMS maps of the inset SP-containing region of (a), recorded on a contiguous section, (b) CN^- map showing the general morphology with better resolution that optical images, (c) P^- map showing the P-rich nucleic acids in nuclei, (d) S^- map showing two granular S-rich regions, A and B; the A region, in the periphery of the SP, is also iron-rich and has been identified as a DN region [23]; B region corresponds to lipofuscin granules present in the cytoplasm of neurons and does not contain iron. Analyzed area of 50μmx50μm.

* Another possibility is the dysfunction of Ft that we have suggested [21,22]. If inappropriate iron sequestration other than ferric Fe^{3+} is produced in these cells, the result is an increase in free ferrous Fe^{2+} iron-induced oxidative stress. The additional presence of Hm in these cells supports this hypothesis, as Hm is considered to be a product of the degradation of Ft and the composition of Hm cores in primary hemochromatosis is similar to wüstite.

The excess of Fe^{2+} due to the dysfunction of Ft may be the cause of myelin damage. Widespread myelin breakdown has been reported in the elderly, and especially in AD [24].

The presence of biogenic ferromagnetic magnetite/maghemite crystals in the extracts from healthy and pathological brains has been described since 1992 [49]. As the brain samples were taken from cadavers, this work proved controversial.

A few years later the Dobson group confirmed and expanded this result also by using magnetic methods of measurement on strictly controlled samples. They showed the presence of ferrimagnetic iron oxide compounds in neurological and neurodegenerative diseases as neurodegenerative diseases epilepsy [50,51] and AD [52]. The ferrimagnetic crystals identified in brain *extracts* were observed by TEM, [49,53], and have a mean diameter of a few tenths of a nm. More recently, and also using magnetic methods, biogenic magnetite/maghemite was found in meningiomas brain tumors and in the hippocampal tissue of patients with mesial temporal lobe epilepsy (MTLE) [54-56] and in basal ganglia of neuroferritinopathy patients [57]. Recently, synchrotron-based techniques, X-ray fluorescence (XRF) and X-ray absorption near edge spectroscopy (XANES), have been used for '*in situ*' detection, identification and mapping of small-scale iron components in the brain [58]. The technique has recently been applied, with a spatial resolution of about *5 μm*, to the study of metal compounds in pigeon brains and human AD brains [58-60]. In addition to ferrihydrite, magnetite and wüstite have been identified in iron-rich inclusions observed in sections of human AD brain by Collingood, Davidson, Mikhaylova, Battich and Dobson*. The confirmation of the presence of wüstite in AD samples through a different analytical method to END is an important result that adds a

* Synchrotron X-ray study of Alzheimr's tissue demonstrated mixed-valence iron oxide accumulation in superior frontal gyrus. In 10th International Conference on Alzheimer's Disease and related disorders. Madrid, July 2006. *Alzheimer and Dementia, **2006**, 2(3,) Suppl. 1, S482.*

new argument to support our hypothesis of the *dysfunction of ferritin*.

Is there a relationship between the biogenic *magnetite/maghemite crystal* observed in brain *extracts* and in *sections* of the human AD brain and the *magnetite nanocrystals* present in some Ft cores in PSP and AD? In 2001, Dobson [61] suggested the hypothesis "that the magnetite nanocrystals present in some Ft cores in PSP and AD, could be the precursors of these biogenic brain magnetite/maghe-mite crystals." Recently, Dobson, Collingood, Davidson, Pankhurst, Mikhaylova, Hautot, Dunin-Borkowski, Posfai, Kasama, Chong and Battich[**] claim to have found, "by HRTEM", magnetite nanocrystals on the *isolated* senile plaques of AD subjects.

CONCLUSION AND PERSPECTIVES

Analytical transmission electron microscopy, like HRTEM, END and EELS, are very useful techniques for the characterization of nanocrystals. Therefore, it is necessary to know their limitations for the study of iron oxides. Magnetite (Fe_3O_4), is a mixed Fe^{2+} and Fe^{3+} iron oxide that cannot be differentiating by HRTEM to maghemite, (γFe_2O_3), a ferric iron oxide with very similar magnetic proprieties. END theoretically allows this differentiation but it requires well characterized standard or complex software for modelling the diffracted intensities. With EELS it is possible to differentiate magnetite from maghemite: from the study of the fine structure of the iron $L_{2,3}$ peak by ELNES (electron-loss-near-edge structure) [31] it is possible to identify the valence state of iron in EELS instruments with a energy resolution better than 1eV at 700 eV. These instruments, mainly associated to a STEM, allow us to identify the iron oxide composition of *individual cores* of isolated Ft molecules deposited on very thin films of carbon, Fig (**5d**).

Application of the ATEM techniques to the compositional studies of Ft core nanocrystals in *sections* of brain is not straightforward because of (1) the small signal/background ratio due to the thickness of sections that are several times greater than the nanocrystal dimension and (2) the contamination of biological samples that weaken the analytical signal. For these reasons, until now, we have not obtained definitive results about the composition of Ft and Hm cores observed '*in situ*' in the AD brain. More work must be performed in this direction to confirm *our hypothesis that an excess of Fe^{2+}-ferritinophatie is the non-specific and age-dependent pathogenic event responsible for ND.*

To confirm this hypothesis, in parallel to ATEM '*in situ*' methods, biochemical analysis of isolated Ft and Hm must be performed. Another interesting experiment to help confirm our hypothesis would be the association of different microscopies (light, electronic (TEM) and ionic (NanoSIMS)) with synchrotron derived spectroscopy (X-ray fluorescence (XRF) and X-ray absorption near edge spectroscopy (XANES), with the aim of identifying the intra-cellular and extra-cellular structures where the different iron oxides have been found [60].

In this review we have tried to show how physical analysis techniques, associated with analytical, electronic and ionic microscopies, can provide new results and new ideas to try to understand the different factors that play a role in the onset and development of NDs such as AD and PSP.

ACKNOWLEDGMENTS

This work was supported by grants BMC2002-00996 from the Dirección General de Investigación (Spain), PR2002-0261 from the Ministerio de Educación, Cultura y Deporte (Spain) and FIS-C03-006 from the Ministerio de Sanidad (Spain).

The author express their gratitude to all the members of the U759 INSERM-Institut-Curie-Recherche-Orsay for the warm reception during my sabbatical stay at the nanoSIMS facility and very specially to Dr. Ting-Di Wu. The author would like to pay homage to Dr Cowley (deceased in 2004) for your crucial contribution at this research**.**

REFERENCES

[1] Christen, Y. *J. Soc. Biol.*, **2002**, *196*(1), 85.
[2] Markesbery, W.R. *Free Rad. Biol. Med*., **1997**, *23*, 134.
[3] Perry, G.; Cash, A.D.; Smith, M.A. *J. Biom. Biotech*., **2002**, *2*(3), 120.
[4] Connor, J.R.; Menzies S.L. *J. Neurol. Sci*., **1995**, *134*(Suppl.), 33.
[5] Smith, M.A.; Harris, P.L.T.; Sayre, L.M.; Perry, G. *Proc. Natl. Acad. Sci. USA*, **1997**, *94*, 9866.
[6] Ke, Y.; Qian, Z.M. *Lancet Neurol*., **2003**, *2*, 246.
[7] Moos, T.; Morgan, E.H. *Ann. N. Y. Acad. Sci*., **2004**, *1012*, 14.
[8] Goodman, L. *J. Nerv. Mental Dis.*, **1953***, 117,* 97.
[9] Chasten, N.D.; Harrison, P. *J. Struc. Biol*., **1999**, *126*, 182.
[10] Grundke-Iqbal, I.; Fleming, J.; Tung, Y.C.; Lassmann, H.; Iqbal, K.; Joshi, J.G. *Acta Neuropathol*., **1990**, *81*,105.
[11] Connor, J.R.; Menzies, S.L.; St Martin, S.; Mufson, E.J. *J. Neurosci.,* **1990***, 27,* 595.
[12] Connor, J.R.; Snyder, B.S.; Arosio, P.; Loeffler, D.A.; LeWitt, P. *J. Neurochem.,* **1995***, 65,* 717.
[13] Curtis, A.R.J.; Fey, C.; Morris, C.M.; Bindoff, L.A.; Ince, P.G.; Chinnery, P.F.; Coulthard, A.; Jackson, M.J.; Jackson, A.P.; McHale, D. P.; Hay, D.; Barker, W.A.; Markham, A.F.; Bates D.; Curtis, A.; Burn, J. *Nat. Genet*., **2001**, *28*, 350.
[14] Crompton, D.E.; Chinnery, P.F.; Fey, C.; Curtis, A.R.; Morris, C.M.; Kierstan, J.; Burt, A.; Young, F.; Coulthard, A.; Curtis, A.; Ince, P.G.; Bates, D.; Jackson, M.J.; Burn, J. *Blood Cells Mol. Dis*., **2002**, *29*, 522.
[15] Vidal, R.; Delisle, M.B.; Rascol, O.; Ghetti, B. *J. Neurol. Sci*., **2003**, *207*, 110.
[16] Vidal, R.; Ghetti, B.; Takao, M.; Brefel-Courbon, C.; Uro-Coste, E.; Glazier, B.S.; Siani, V.; Benson, M.D.; Calvas, P.; Miravalle, L.; Rascol, O.; Delisle, M.B. *J. Neuropathol. Exp. Neurol*., **2004**, *63*, 363.
[17] Schröder, J.M. *Acta Neurophathol.,* **2005***, 109,* 109.
[18] Levi, S; Cozzi, A.; Arosio, P. *Best Pract. Res. Clin. Haematol.,* **2005***, 18,* 265.
[19] Perez, M.; Valpuesta, J.M.; Montejo de Garcini, E.; Quintana, C.; Arrasate, M.; Lopez-Carrascosa, J.L.; Rabano, A.; Garcia de Yebenes, J.; Avila, J. *Am. J. Pathol*., **1998**, *152*, 1531.
[20] Rubenstein, R.; Kascsak, RJ.; Merz, P.A.; Wisniewski, H.M.; Caro, R.I.; Iqbal, K. *Brain Res*., **1986**, *372*, 80.
[21] Quintana, C.; Lancin, M.; Marhic, C.; Pérez, M.; Martin-Benito, J.; Avila, J.; Lopez-Carrascosa, J.L. *Cell. Mol. Biol*., **2000**, *46*(4), 807.
[22] Quintana, C.; Cowley, J.M.; Marhic, C. *J. Struct. Biol*., **2004**, *147*, 166.
[23] Quintana, C.; Bellefqih, S.; Laval, J.Y.; Guerquin-Kern, J.L.; Wu, T.D.; Avila, J.; Ferrer, I.; Arranz, R.; Patiño, C. *J. Struct. Biol*., **2006**, *153*, 42.
[24] Bartzokis, G. *Neurobiol. Aging*, **2004**, *25*, 5.
[25] Iancu, T.C. *Electron Microsc. Rev*., **1992**, *5*, 209.
[26] Cowley, J.M. *Diffraction Physics*. North-Holland Physics Publishing: Amsterdam, **1984**.
[27] Cowley, J.M. *Micron,* **2004***, 35,* 345.

[**] Iron and Alzheimer disease: new insights from novel imaging techniques. In 10th International Conference on Alzheimer's Disease and related disorders. Madrid, July 2006. *Alzheimer and Dementia, **2006**, 2(3,) Suppl. 1, S482.*

[28] Quintana, C. ; Bonnet, N. ; Jeantet, A.Y. ; Chemel, P. *Biol. Cell*, **1987**, *59*, 247.
[29] Janney, D.E.; Cowley, J.M.; Buseck, P.R. *Am. Mineral*., **2000**, *85*, 1180.
[30] Cowley, J.M.; Janney, D.; Gerkin, R.C.; Buseck, P.R. *J. Struct. Biol.*, **2000**, *131*, 210.
[31] van Aken, P.A.; Liebscher, B.; Styrsa, V.J. *Phys. Chem. Minerals,* **1998**, *25,* 323.
[32] Guerquin-Kern, J.L.; Wu, T.D.; Quintana, C.; Croisy, A. *Biochim. Biophys. Acta, General Subjects*, **2005**, *1724*, 228.
[33] Quintana, C.; Wu, T.; Delatour, B.; Dhenain, M.; Guerquin-Kern, J.L.; Croisy, A. *Microsc. Res. Tech*., **2007**, *70*, 281.
[34] Towe, K.M.; Bradley, W.F. J. *Colloid. Interface Sci*., **1967**, *24*, 384.
[35] Harrison, P.M.; Fischbach, F.A.; Hoy, T.G.; Haggis, G.H. *Nature,* **1967**, *216,* 1188.
[36] Heald, S.M.; Stern, E.A.; Bunker, B. J. *Am. Soc.,* **1979**, *101,* 67.
[37] Massover, W.H.; Cowley, J.M. *Proc. Natl. Acad. Sci. USA*, **1973**, *70*, 3847.
[38] Isaacson, M.S.; Ohtsuki, M. *Scannig Electr. Microsc*., **1980**, *1*, 73.
[39] Eggleton, R.A.; Fitzpatrick. R.W. *Clays Clay Minerals,* **1988**, *36,* 111.
[40] Drits, V.A.; Saharov, A.L.; Salyn, A L.; Manceau, A. *Clay Minerals*, **1993**, *28*,185.
[41] Jambor, J.L.; Dutrizac, J.E. *Chem. Rev*., **1998**, *98*, 2549.
[42] Janney, D.E.; Cowley, J. M.; Buseck, P. R. *Am. Mineralogist*., **2001**, *86*, 327-335.
[43] Dickson, D.P.E.; Reid, N.M.K.; Mann, S.; Wade, V.J.; Ward, R.J.; Peters, T.J. *Biochem. Biophys. Acta,* **1998**, *957,* 81.
[44] Connor, J.R.; Milward, E.A.; Moalem, S.; Sampietro, M.,; Boyer, P.; Percy, M.E.; Vergani, C.; Scott, R.; Chorney, M. *J. Alzh. Dis.,* **2001**, *3,* 471.
[45] Sampietro, M.; Caputo, L.; Casatta, A.; Meregalli, M.; Pellagatti, A.; Tagliabue, J.; Annoni, G.; Vergani, C. *Neurobiol. Aging*, **2001**, *22*, 563.
[46] Bartzokis, G.; Tishler, T.A.; Shin, I.S.; Lu, P.H.; Cummings, J.L. *Ann. N. Y. Acad. Sci*., **2004**, *1012*, 224.
[47] Heywood, B.R.; Bazylinski, D.A.; Garret-Reed, A.; Mann, S; Frankel, R.B. *Naturwissenschaften,* **1990**, *77,* 536.
[48] Kasama, T.; Pósfai, M.; Chong, R.K.K.; Finlayson, A.P.; Dunin-Borkowski, R.E.; Frankel, R.B. *Physica B: Condensed Matter*, **2006**, *384*, 249.
[49] Kirschvink, J.L.; Kobayashi- Kirschvink, A.; Woodford, B.J. *Proc. Natl. Acad. Sci. USA*, **1992**, *89*, 7683.
[50] Dunn, J.R.; Fuller, M.; Zoeger, J.; Dobson, J.; Heller, F.; Hammann, J.; Caine, E.; Moskowitz, B.M. *Brain Res. Bull*., **1995**, *36*, 149.
[51] Schultheiss-Grassi P.P.; Dobson J. *Biometals*, **1999a**, *12*, 67.
[52] Hautot, D.; Pankhurst, Q.A.; Khan, N.; Dobson J. *Proc. R. Soc. Lond. B (Suppl.)*, **2003**, DOI 10.1098/rsb1.2003.0012.
[53] Schultheiss-Grassi, P.P.; Wessiken, R.; Dobson, J. *Biochim. Biophys. Acta*, **1999b**, *1426*, 212.
[54] Brem, F.; Hirt, A.M.; Simon, C.; Wieser, H.G.; Dobson, J. *J. Physics Conf. Ser.*, **2005a**, *17*, 61.
[55] Brem F.; Hirt, A.M.; Simon, C.; Wieser, H.G.; Dobson, J. *Biometals*, **2005b**, *18*, 191.
[56] Brem, F.; Hirt, A.M.; Winklhofer, M.; Frei, K.; Yonekawa, Y.; Wieser, H.G.; Dobson, J. *J. R. Soc. Interface*, **2006**, *3*, 833.
[57] Hautot, D.; Pankhurst, Q.A.; Morris, C.; Curtis, A.; Burn, J.; Dobson, J. *Biochim. Biophys. Acta*, **2007**, *1772*, 21-5.
[58] Mikhaylova, A.; Davidson, M.R.; Toastman, H.; Channell, J.E.T.; Guyodo, Y.; Batich, C.; Dobson, J. *J. R. Soc. Interface*, **2005**, *2*, 33.
[59] Collingwood, J.F.; Mikhaylova, A.; Davidson, M.R.; Batich, C.; Streit, W.J.; Eskin, T.; Terry, J.; Barrea, R.; Underhill, R.S.; Dobson, J. *J. Physics: Conference Series*, **2005a**, *17*, 54.
[60] Collingwood, J.F.; Mikhaylova, A.; Davidson, M.R.; Batich, C.; Streit, W.J.; Terry, J.; Dobson, J. *J. Alzheimers Dis*., **2005b**, *7*, 267.
[61] Dobson, J. *FEBS Lett.*, **2001**, *496*, 1.

Received: 05 December, 2006 Revised: 16 March, 2007 Accepted: 16 March, 2007